Research Article ISSN 2832-9384

Journal of Materials and Polymer Science

Corrosion Investigation with Focused Ion Beam and SEM Technology

Christian Paglia

University of Applied Sciences of Southern Switzerland, DACD, V. F. Ruchat 15, 6850 Mendrisio, Switzerland.

***Corresponding author**

Christian Paglia,
University of Applied Sciences of Southern Switzerland, DACD, V. F. Ruchat 15, 6850 Mendrisio, Switzerland.
ORCID : https://www.researchgate.net/profile/C-Paglia

Submitted : 6 Dec 2024 ; Published : 10 Jan 2025

Citation: Paglia, C. (2025). Corrosion Investigation with Focused Ion Beam and SEM Technology. *J mate poly sci, 5*(1) :1-11.
DOI : https://doi.org/10.47485/2832-9384.1068

Abstract
A strong relationship exists between the properties of the materials and the microstructure. Within the metals, small changes in the heat treatments, may significantly affect the microstructure. Consequently, the mechanical characteristics change. The microstructure also influence their corrosion behavior. The main diagnostic techniques allow the observation of surface events. Nonetheless, a simultaneous relation to the depth gives considerable information on the severity, the penetration and the extent of localized corrosion. Furthermore, the interaction between the metal surface and the main protection systems, such as coating, is a key issue to get durable structures. The focused ion beam FIB and SEM technology proved to be useful for the in-situ characterization of corrosion related issues. The FIB cross sections of pits, intermetallic particles and coatings give additional microstructural information on localized corrosion as well as on the coating / metal interface, which are not always evident to detect with conventional diagnostic techniques.

Keywords: FIB, SEM, metal alloys, cross sections, corrosion.

Introduction

The versatility of the FIB and SEM technology allows various applications, such as micro-machining (Ishitani et al., 1991), repair of integrated circuits (Komano et al., 1991), failure analysis (Nikawa, 1991, Kirk et al., 1988), TEM sample preparation (Young et al., 1990), and investigations of superconductors (Kern et al., 1991). The FIB is similar to the field emission scanning electron microscopes (FESEM). These instruments are based on charged particle beam, which are rastered across a solid surface, producing high resolution images. In the FIB, the charged particles are gallium ions, while in the FESEM are electrons. In the FIB, however, the mass of the charged species is significantly high, so that the interaction of the gallium ions with the surface is accompanied by the sputtering of the surface (Presser & Hilton, 1997). The combination of sputtering and high resolution allows in-situ microscopic milling and machining of the surface, which can then be observed with SEM (Presser & Hilton, 1997). The principles of micro-machining and micro-deposition of the FIB were already described (Davis & Khamsehpour, 1996).

The FIB cross sections generally enable the characterization of oxide film morphology (Presser & Hilton, 1997; Heilmann et al., 1999), and were used to investigate Raney copper® (Smith et al., 1999). However, the applicability of this technique accompanied with SEM in the corrosion field was not yet established. In this work, localized corrosion features as well as the coating morphologies were studied with FIB cross sections to clarify the capability of the FIB technique to reveal additional microstructural information as compared to conventional techniques.

Experimental Procedure

The Workstations

The dual beam device integrates ion and electron beams for FIB and SEM functionality. Convergence of SEM and FIB at short working distance allows “slice and view” cross section points, which are set to the eucentric point, where the feature of interest remains in focus after rotation or stage title (xP Dualbeam Workstation User’s Guide, 2003). Images view in secondary ion or electron mode are possible (Fig. 1). The FIB consists of a MagnumTM ion column providing precise milling and high-resolution images of the sample surface. The SEM column (HexalenTM) allows image resolution at low beam energies magnified over 500 kX in search mode and greater than 2500 kX in UHR mode. The workstation chamber allows to accomodate up to 200 mm samples in a high-vacuum environment. The Gas Injection System uses Enhanced EtchTM for fast material removal with minimal re-deposition, as well as metal deposition (xP Dualbeam Workstation User’s Guide, 2003). In the present investigation, the pictures were imaged in a E-beam mode (5 kV) where not specified, otherwise in a I-beam mode (30 kV). The desktop SEM consisted of a

Thermo Scientific Phenom XL G2 with EDX - SED for spot, line and imaging with a scanning area of 100 mm x 100 mm.

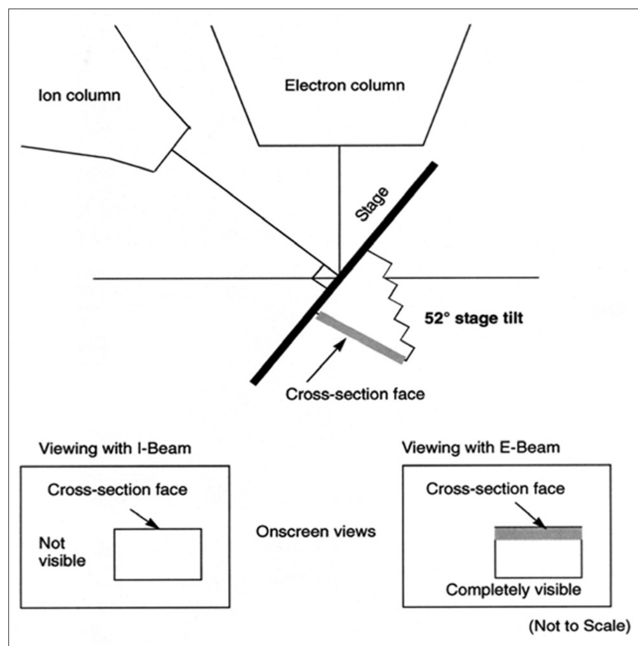

Figure 1

Samples

The FIB samples are prepared as for conventional SEM devices. In the present work, the dealloying of the Al_2CuMg particles was carried out by immersing a 2024-T3 aluminium alloy to an aerated 0.1 M NaCl solution for 5.5 hours. A 7075-T6 aluminium alloy exposed for 2 minutes in an aerated 3.5 % NaCl solution was used to investigate the pits and the anodic dissolution of the intermetallics, while the intergranular attack of a 7075-T6 aluminium alloy was studied by polarizing the samples above –0.800 V for 24 hours. For the investigation of layered structures, a chromate conversion coating was applied to a 2024-T3 AA by immersing the samples in Alodine 1200S solution (Material Safety Data Sheet for Alodine 1200S, 1997), whereas a sol-gel conversion coating was applied to a 3004 AA. The aluminium coating on a copper substrate was deposited with the flash evaporation method (Maissel & Glang, 1970). The degradation of the electronic components was studied by exposing the specimen in a 100 % relative humidity for 3 months.

Results and Discussion

Cross Section Optimization

The FIB cross sections are usually done by tilting the stage to 52° with respect to the horizontal stage line as depicted in Fig 1. In this case, the ion beam is perpendicular to the sample surface and mills it. However, when the sample surface is kept horizontal, a slanted cut through the material is obtained (Fig. 2). In this latter case, the morphological features of the cross section face, such as oxide layers, porosity, corrosion products and particle redistributions are accentuated in their dimensions. Cutting with a zero stage tilt does not generally affects the precision of the milling procedure. Moreover, tilting back the cross section face to the horizontal position enables clear EDAX measurements (Fig. 2) with no rays reflection from other portions of the milling area. This last stage adjustment allows to perform chemical mapping of the sample along the cutting edge, gaining informations on the chemical composition with depth. Nonetheless, in order to get signals only from the cross section face, enough large bulk mill and platinum layer deposition behind the cross section face is advised (xP Dualbeam Workstation User's Guide, 2003). Milling was generally carried out with a 500 pA aperture and accelerating voltage of 30kV. Too high currents were avoided in order to decrease excessive damage of the surface, which is pronounced in aluminium alloys. In this concern, it was necessary to find a reasonable balance between time, ion current intensity and the area to be investigated.

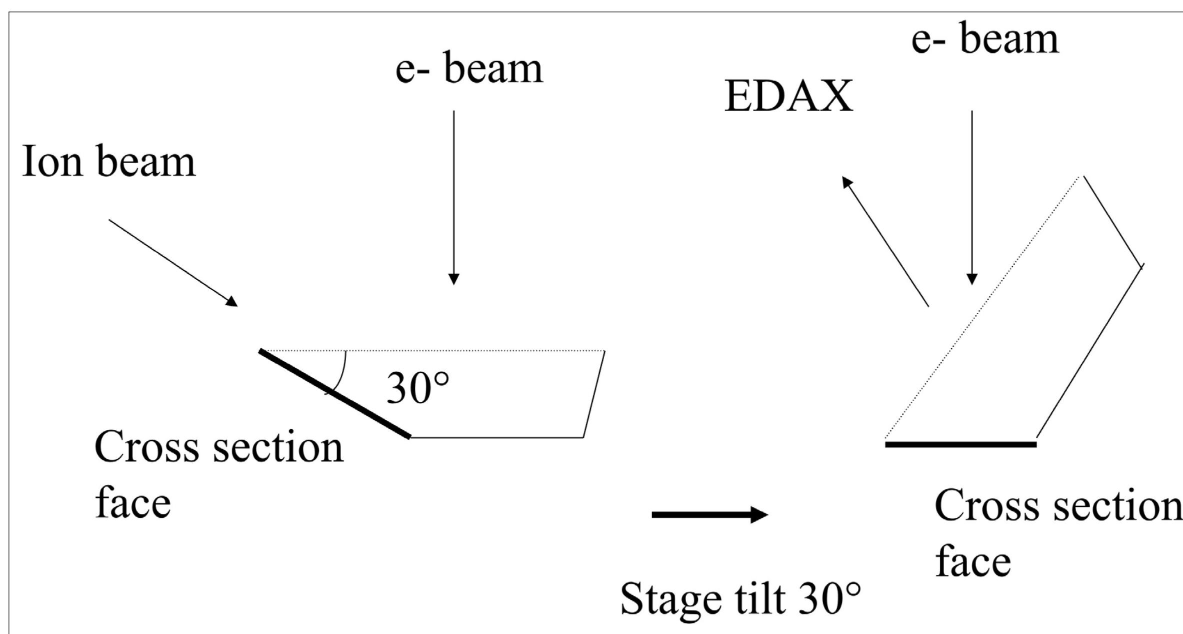

Figure 2

The deposition of a platinum layer on the surface (Fig. 3) stabilizes the cut milling procedure with respect to the cross section face. The platinum largely reduces the curtain-like artifacts and decreases the material transport towards the bottom of the engraving. The sample area is protected from removal of material caused by the impact of heavy ions onto the surface. If no platinum layer is deposited, large curtain-like effects with a large material transport towards the bottom of the cutting area is seen (Fig. 4a, b). Moreover, the cutting area is exposed to the heavy gallium ions, which largely modify the cross section surface with the formation a wave-like features (Fig. 4b).

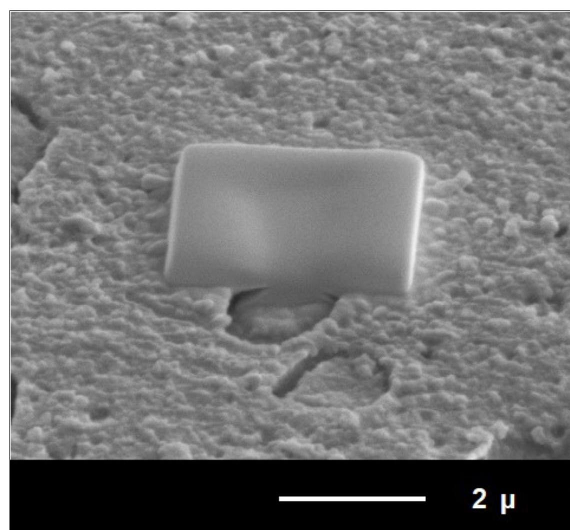

Figure 3

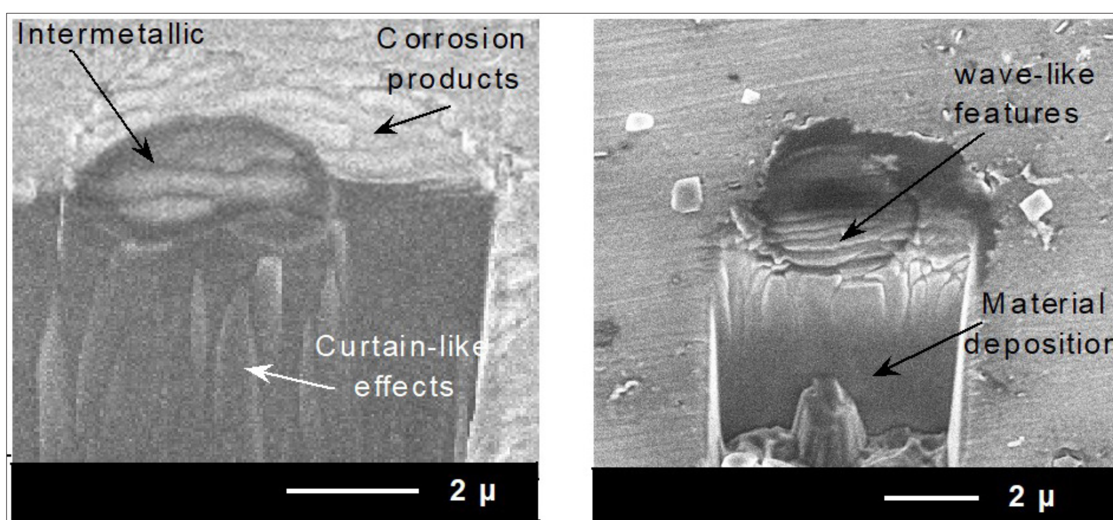

Figure 4

The platinum deposition is doing by heating a methyl-cyclo-pentadienyl trimethyl platinum for ca.10 minutes at temperatures between 38-42°C. The deposition is a balance between decomposing the adsorbed gas and sputtering (xP Dualbeam Workstation User's Guide, 2003). The deposition current is calculated assuming 4 pA/µm2 as a reference value and must be multiplied with the area to be sputtered. Using the calculated value as a threshold current limit reduces the damage probability of the surface due to an excess in the deposition current. However, for the investigation of very thin (nm range) oxide layer or coatings, a thin Pt layer pre-deposition with the electron beam mode should advance the Pt ion beam deposition in order to avoid any adverse interaction of the gallium ions with the surface. The electron beam mode deposition is more time consuming. In the present investigations, an average deposition current of about 1000 pA, and a Pt layer thickness of 1 µm were used. Depending on the topographic features and the area to be analysed, the Pt thickness as well as the deposition current can be adjusted accordingly. The beneficial effect of Pt in stabilizing the cross section cut is lowered if the thickness of the layer is too high. In this case additional material might be transported towards the bottom of the cutting region masking the features to be investigated (Fig. 5).

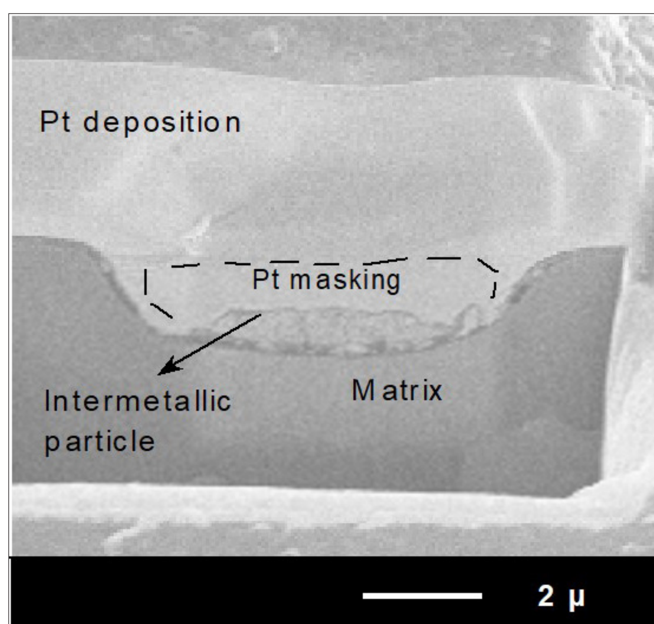

Figure 5

As for solid state devices (Matsui & Ochiai, 1996), cleaning cuts eliminate curtain-like effects along the cross section face (Fig. 6). In fact, series of advancing cutting lines "shave" the face of the cross section (xP Dualbeam Workstation User's Guide, 2003) finely removing the material, enabling a better identification of the microstructural features.

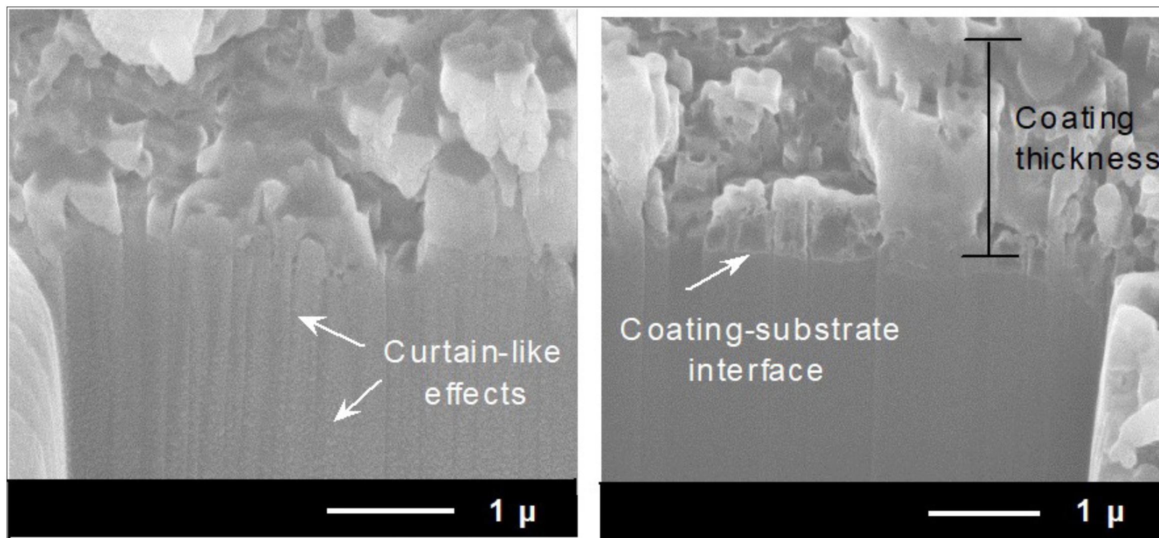

Figure 6

Localized Corrosion

Intermetallic particles play a decisive role in localized corrosion of aluminium alloys (Buchheit et al., 2001). The investigation of dealloying for s-phase particles within Al-Cu alloys exposed to NaCl solution indicates Cu-rich remnants (Buchheit et al., 1997; Obispo et al., 2000). The FIB technique gives additional insights on the dealloying and morphology of Al2CuMg particles, which are generally investigated with SEM (Dimitrov et al., 2000; Wagner et al., 1997).

In order to stabilize the milling procedure for the fragile Al2CuMg intermetallics, a platinum layer was deposited on the particles so that part of it could still be visible. In this manner, a very precise targeting of the area to be milled could be achieved (Fig. 7).

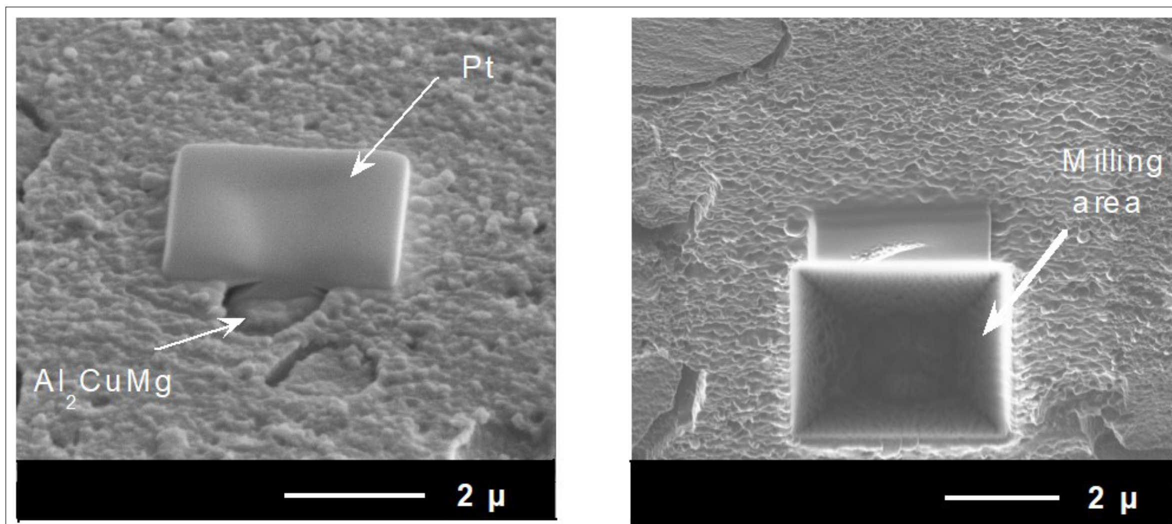

Figure 7

Conventional SEM investigation exhibits dealloying of the particle surface with the formation of Cu clusters (Fig. 8a). After FIB sectioning, the particle shape is maintained and a fully penetrated dealloying is seen (Fig. 8b). The cross section face shows a two-phase solid-void corrosion morphology as already seen (Sieradzki & Newman, 1987; Li & Sieradzki, 1992) above the critical potential. The FIB indicates ion dissolution within the whole particle enabling a full penetration of the dealloying process with depth. A vertical mass transport with a coarsening of the ligaments towards the bottom of the intermetallics was observed after FIB cross sections (Buchheit et al., 2001) and was related to a later stage dealloying. With less aggressive exposure conditions, the FIB presumably enables to directly follow the dealloying front within the Al2CuMg intermetallics giving important informations on the dealloying kinetic.

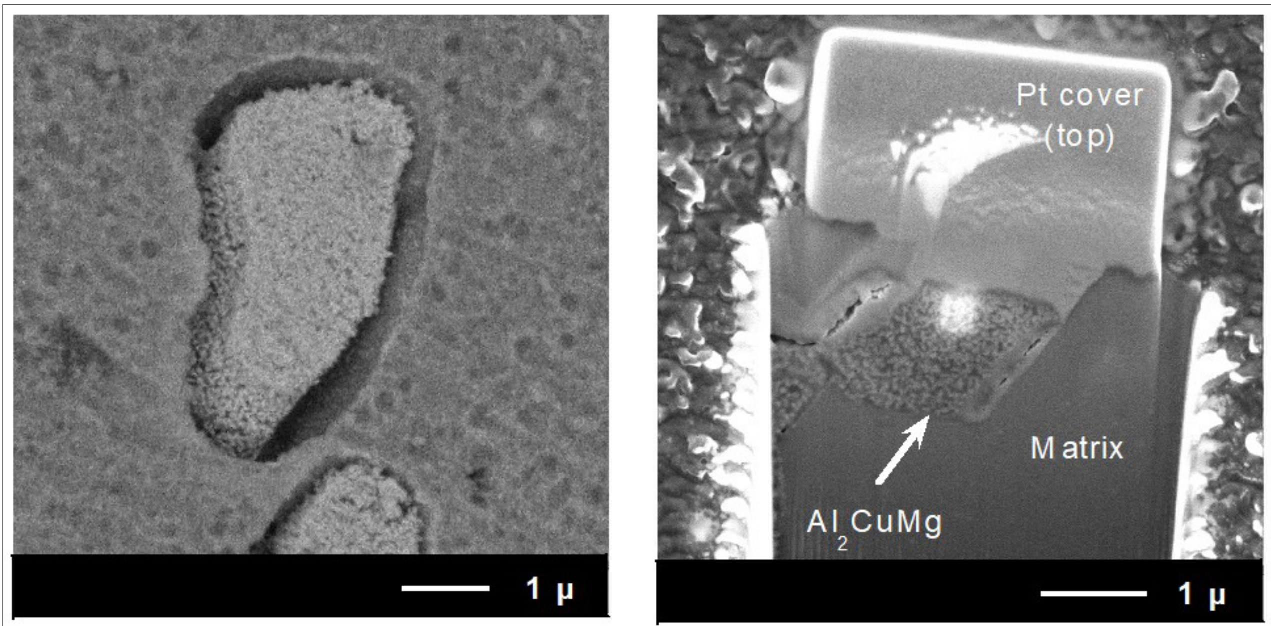

Figure 8

The anodic dissolution of intermetallics, within a 7075-T6 AA exposed for 2 minutes in an aerated 3.5 % NaCl solution, is also detected with a 2-D SEM image mode (Fig. 9a). An early-stage homogeneous dissolution of the intermetallic takes places. This dissolution is limited to the upper surface levels. Nonetheless, FIB cross section slices (ca. 600 nm for each step) through the corroded area of the intermetallic reveal that the corrosion already penetrated to a deep level (Fig. 9b 2,4). This indicates that corrosion in the vertical direction may sometimes proceed to a much faster rate than it appears from 2-D micrographs. Depending on the cross section position on the dealloyed area, the extent of the corrosion penetration significantly changes (Fig. 9b 2-6). These latter observations cannot be recognized with a conventional 2-D image, which exhibits an apparent uniform corrosion of the dealloyed area (Fig. 9a).

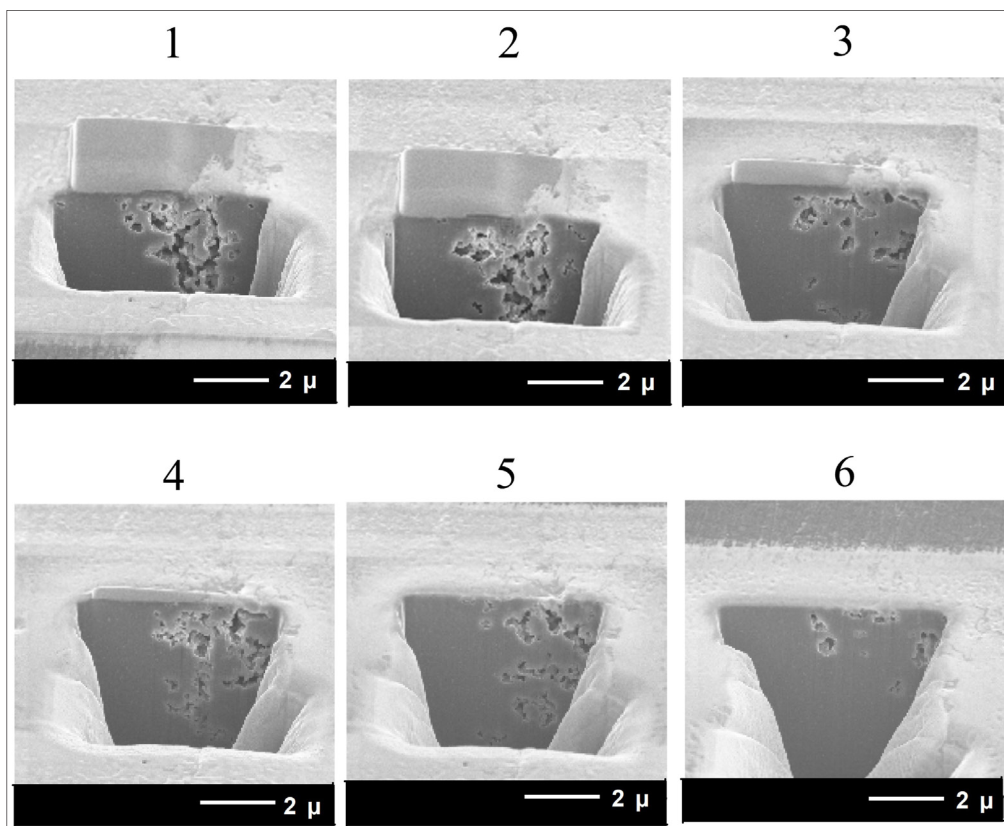

Figure 9

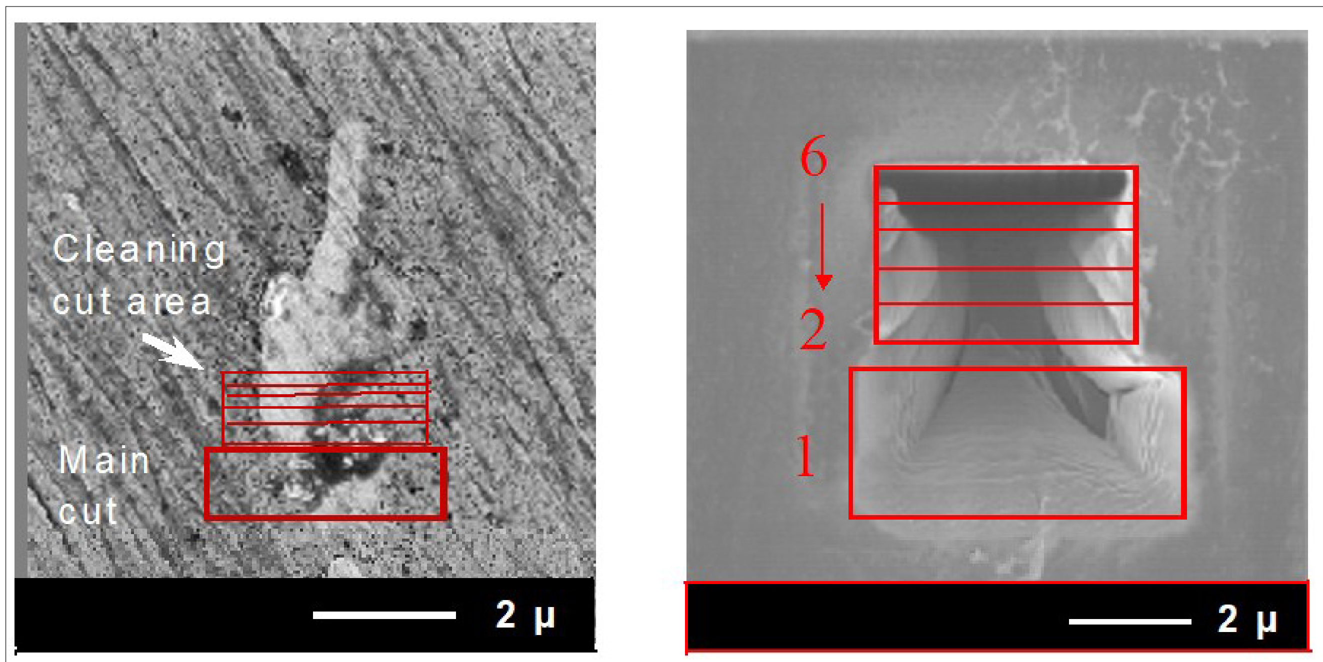

Figure 9 a

Pits also occur on the metals surface. The FIB cross section of a pit without platinum deposition shows the distribution of the localized corrosion underneath the pit, presumably revealing the transition pit-intergranular attack with depth (Fig. 10).

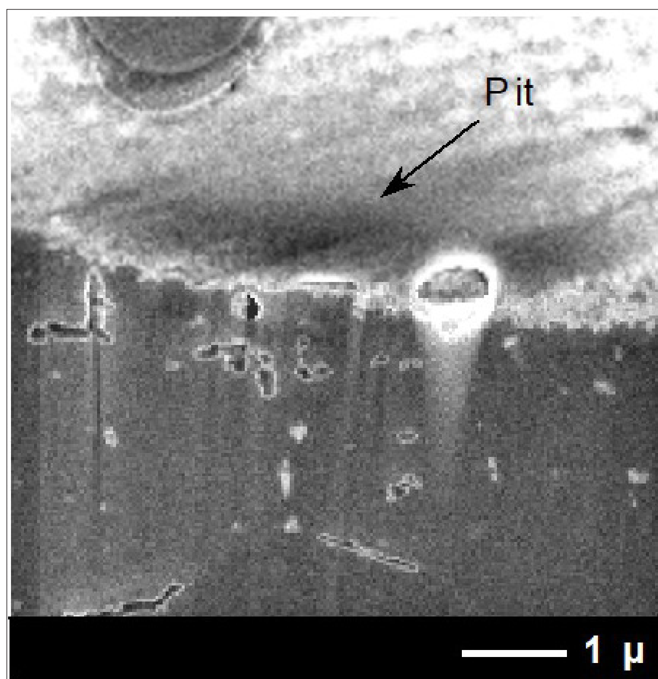

Figure 10

The FIB technique exhibits its investigation's capability of 7075-T6 intergranular corrosion. By applying a potential above –0.800 V (Pitts et al., (in press)), intergranular attack is seen (Fig. 11a, 12a). It initiates with regions of localized dissolution along grain boundaries (Fig. 10a). In this initial stage, the attack is sharp and limited along the grain boundaries, but proceeds within the grain interior at a later stage with the formation of a dissolution front along the grain boundary (Fig. 11b, c). Within highly corroded regions, the grains almost completely dissolve with the formation of large microstructural pits close to the surface.

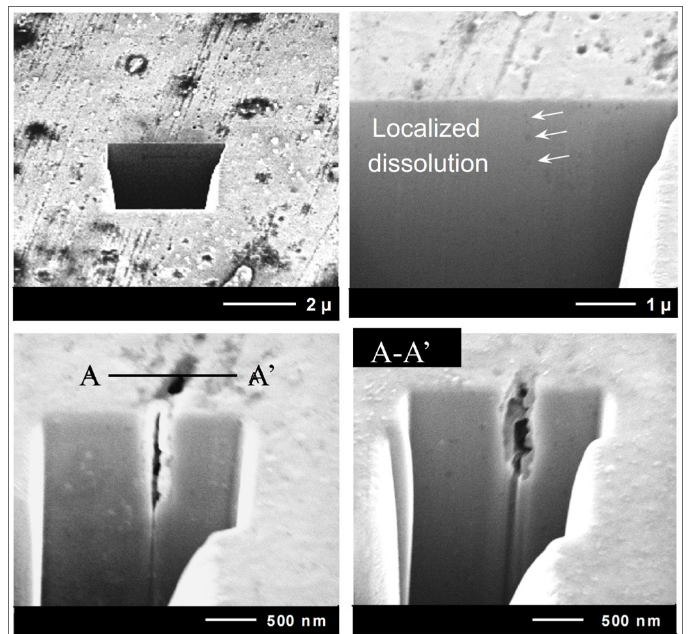

Figure 11

The intergranular degradation below the microstructural pit proceeds with a sharp attack located along the grain boundary (Fig. 12b) and presumably widen again towards the grain interior.

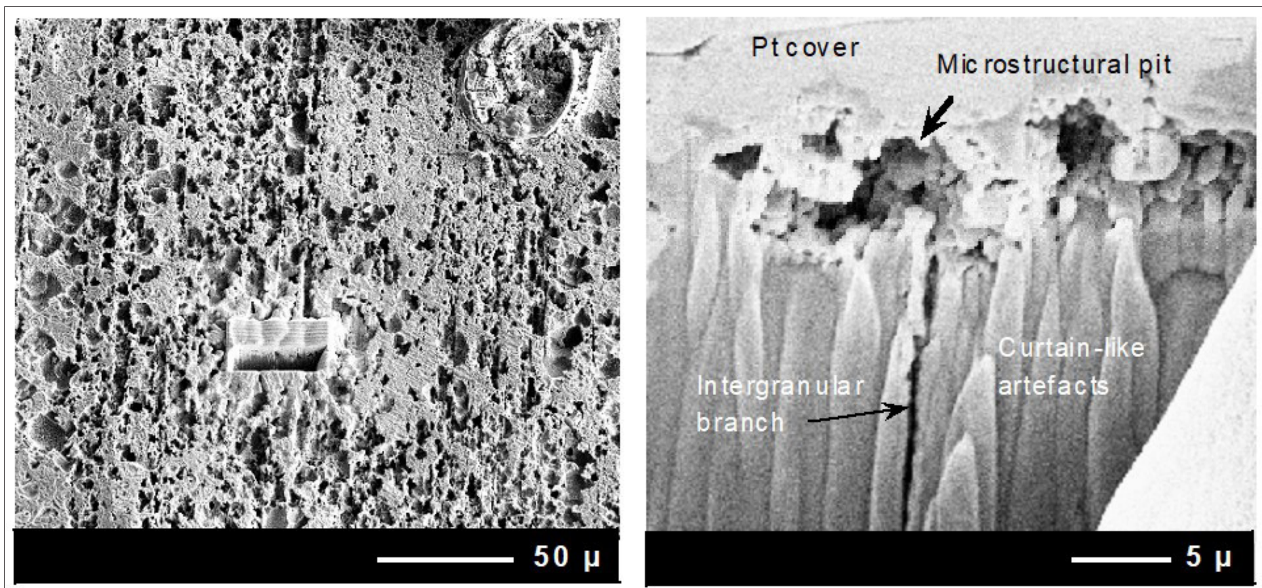

Figure 12

Coatings

Layered structures can be directly analyzed and cross sectioned with the FIB technique as long as they are protected from the impact of the heavy gallium ions during the cutting procedure (platinum deposition). The only limiting factor is the SEM resolution. The low thickness of coatings requires the deposition of a platinum layer. With the FIB the coating microstructure and thickness (Fig. 13 a, b) can be seen.

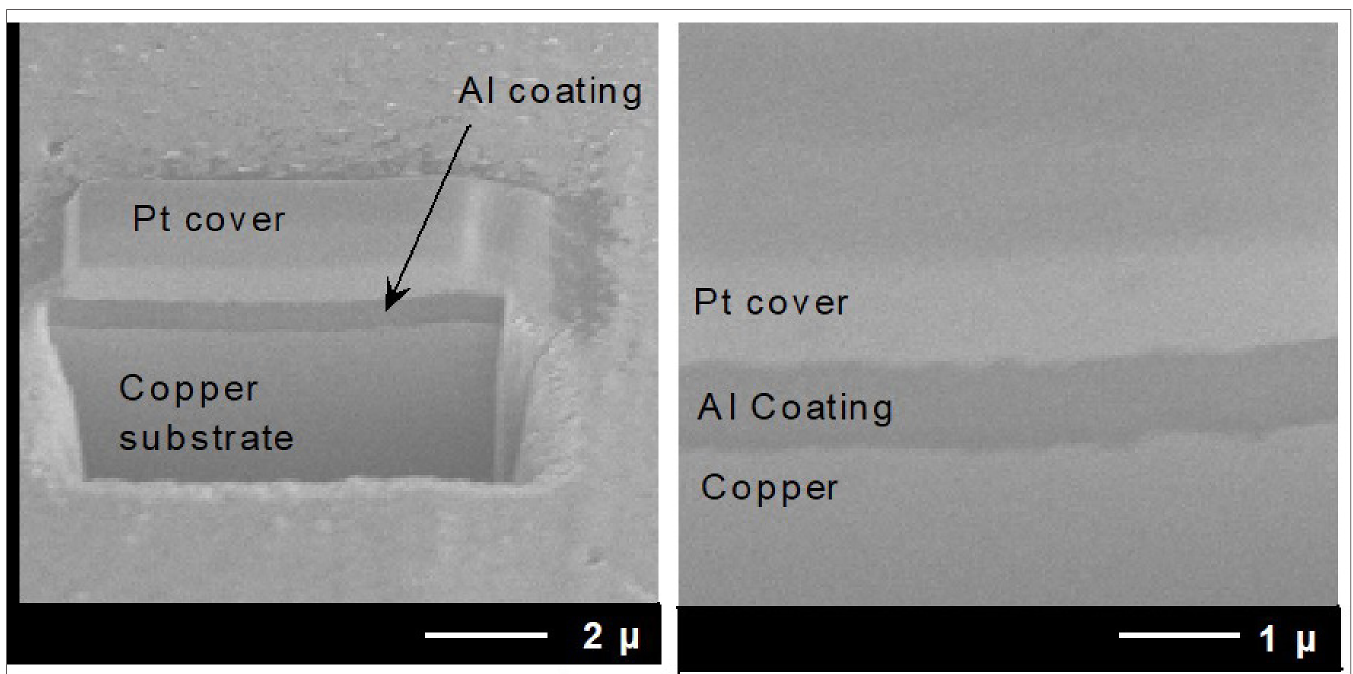

Figure 13

The metal-coating interface can also directly be investigated (Fig. 14).

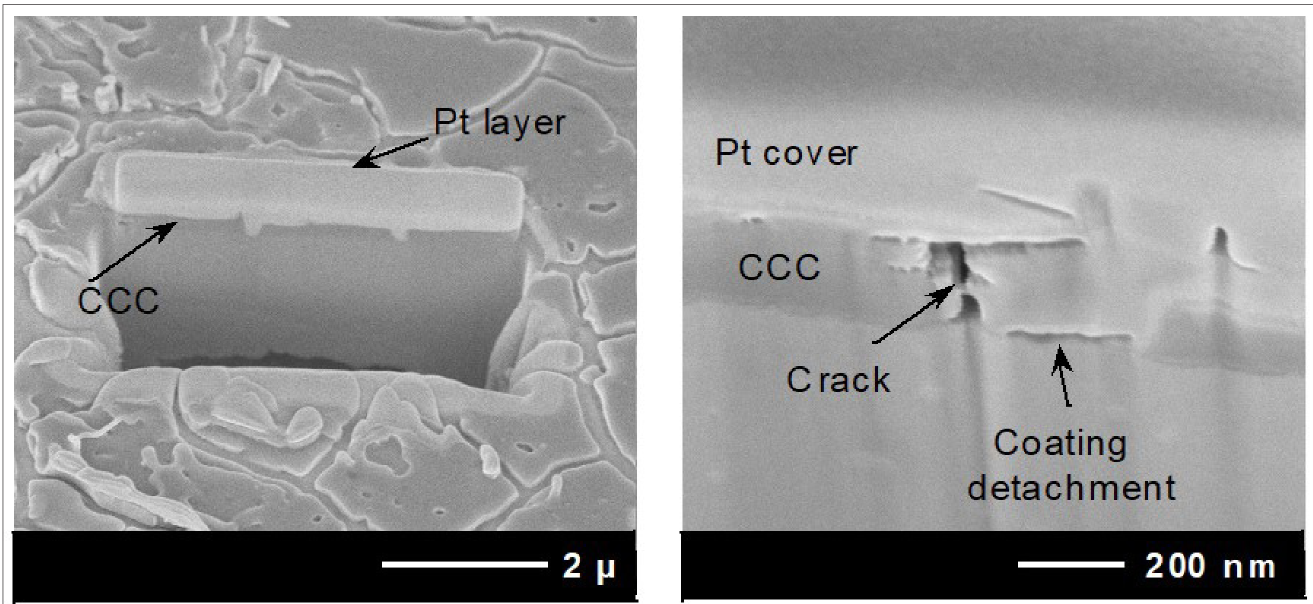

Figure 14

Chromate Conversion Coatings (CCC) were largely investigated in the corrosion of aluminium alloys because of their protection action [Kendig et al., 1999; Llevbare et al., 2000; Pocock, 1954; Sakashita & Sato, 1979; Sato, 1989) and their self-healing mechanism (Glass, 1968). Many examinations of CCC coatings were done with surface sensitive techniques (Arrowsmith et al., 1984; Treverton& Davies, 1977), but additional insights along the coating-metal interface can be gained with the FIB.

A mud-crack-like morphology is seen for the 300 nm thick CCC due to its dehydration and shrinkage during drying (Fig. 14a). The FIB cross sections reveal that the cracks on the surface are not only limited in the outer layer region, but may penetrate until the metal interface (Fig. 14b). The cracks penetration until the metal substrate is not always clear by observing the coating with conventional SEM techniques. Isolated regions of coating detachment, which were not generated from surface cracks were are also found. However it is difficult to explain if the isolated coating detachments are the result of a coating shrinkage or due to the chromating technique.

Additional informations on the FIB cross section faces is gained for a coating applied on 3004 AA. In fact, in a 2-D SEM image mode, the coating appears as a dense and homogeneously distributed layer covering the metal substrate (Fig. 15a). After FIB cross sectioning discontinuous 500 nm capillary pores occasionally reach the metal substrate (Fig. 15b).

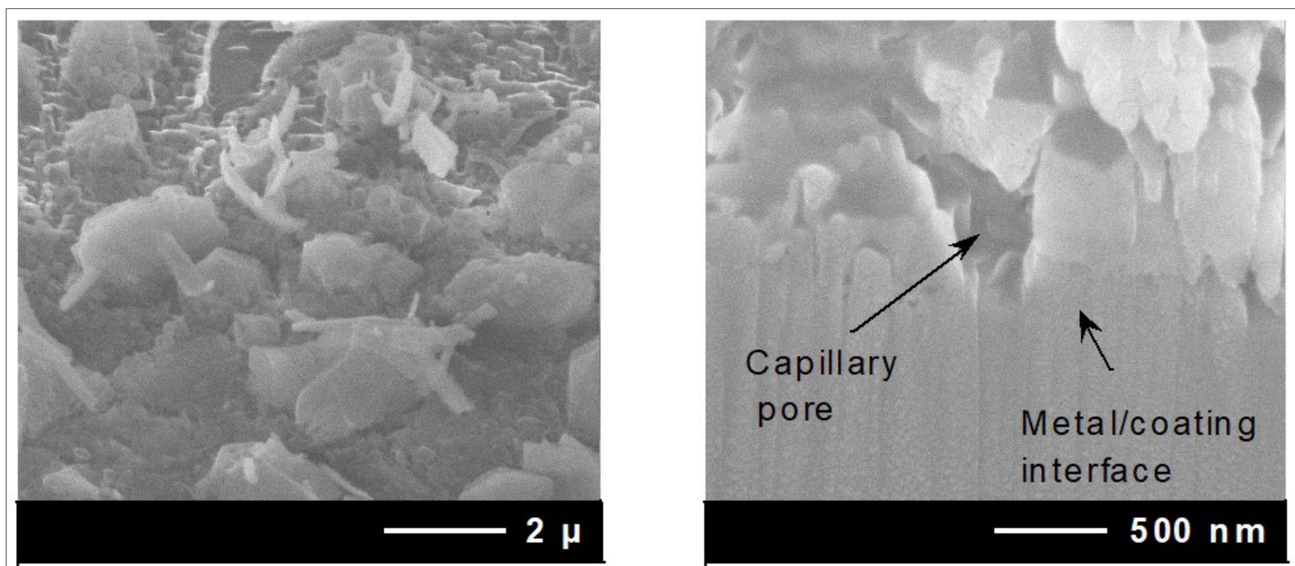

Figure 15

Electronic Component

Electronic components are critical with respect to the humidity. Corrosion features are often not so easy to be detected, apart from the current interruption of the device. Soldering of the elements as well as the layered metallic structures play a relevant role in the degradation (Judd & Brindly, 1992; Coombs, 1995). Component's edge degradation and cracking is often observed (Fig. 16).

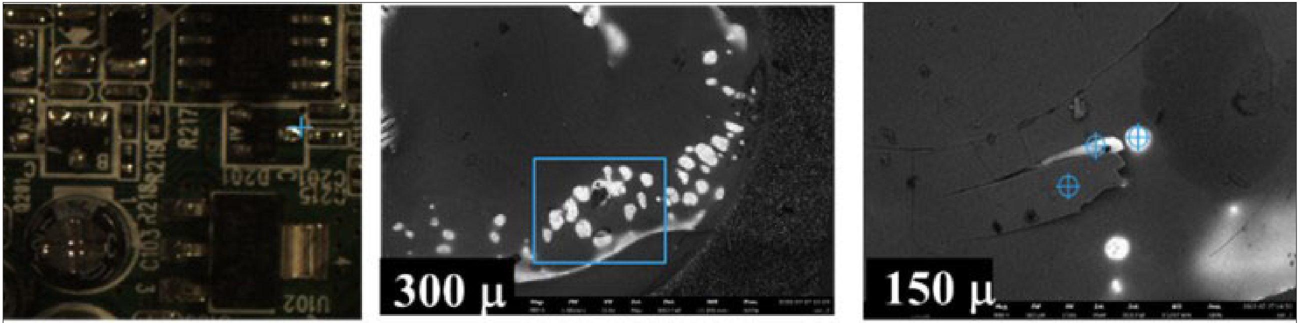

Figure 16: Localized dissolution and cracking along the edges.

The shaping of the elements may create curvatures that promote thinning and degradation along the edges (Fig. 17).

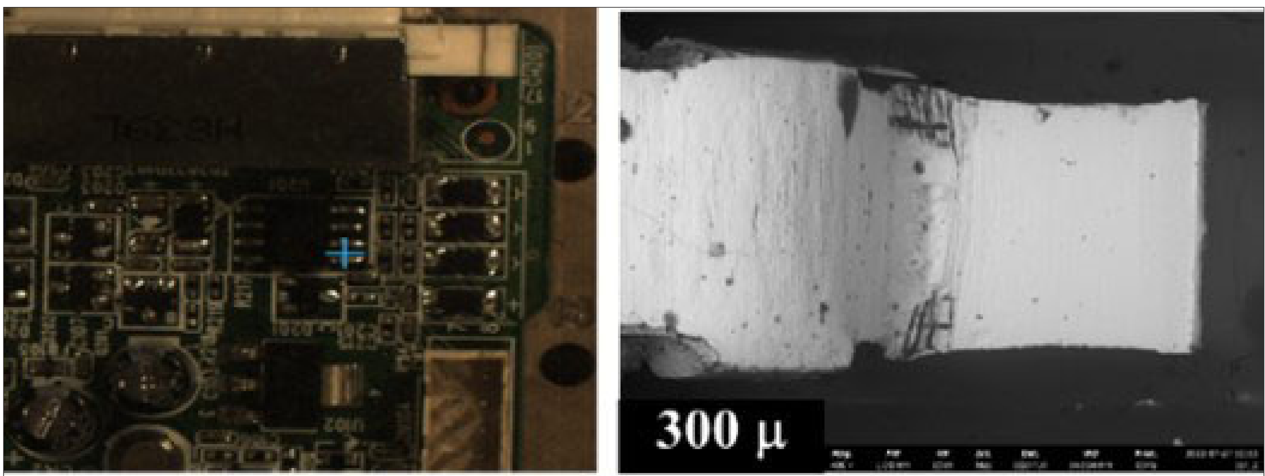

Figure 17: Curvature and metal cover thinning.

Grained and fine cracked rough surface is seen on AA components (Fig. 18 left, centre-left), while a localized dissolution is found for an Sn-Ag-Si alloy (Fig. 18 centre-right, right).

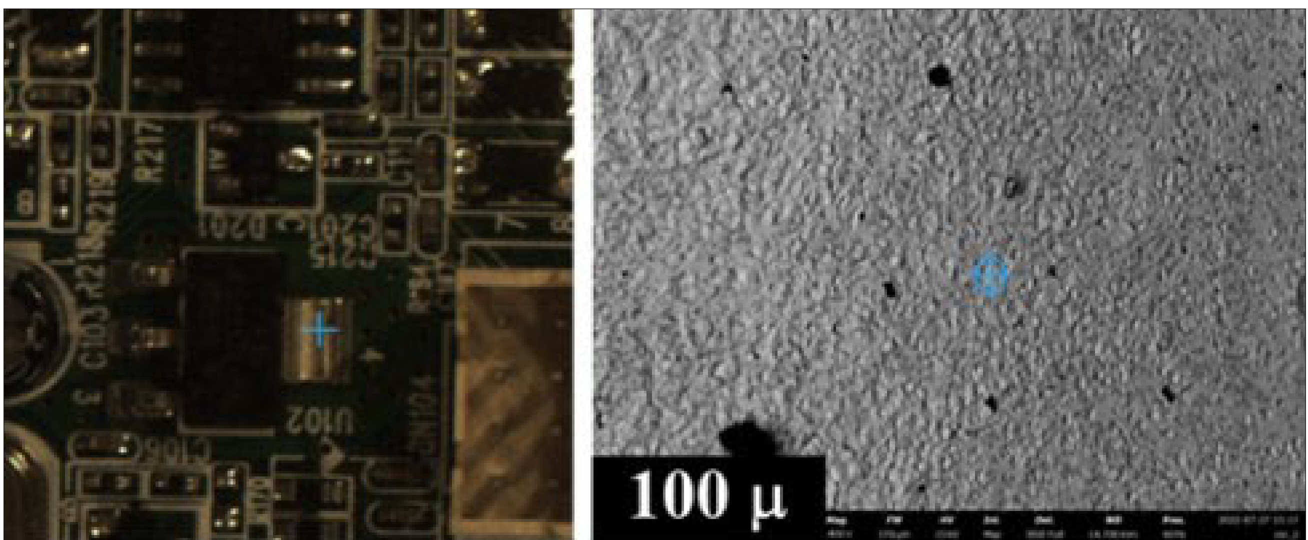

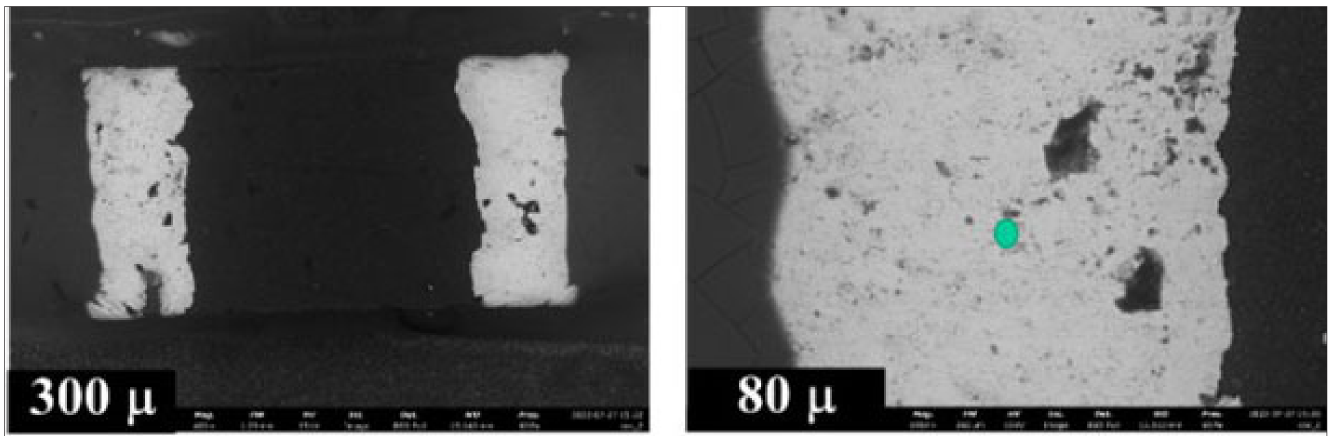

Figure 18: Crack and local dissolution on electronic alloy components.

Conclusions

The FIB and SEM technique supports the conventional investigation of localized corrosion, such as dealloying kinetic, vertical material transport and dealloying fronts within intermetallics, degree of dissolution within intermetallics with depth as well as intergranular attack mechanisms, coating thinning and edge components degradation. The FIB cross section of coatings also reveal additional information, such as coating structure, thickness and the metal-coating interface, which may be used to understand and predict corrosion. The dual beam device (SEM-FIB) and the SEM are useful tools for the in-situ investigation of the corrosion of aluminium alloys and electronic components and gives additional information with depth, which are not evident with conventional instruments.

Acknowledgements

The author would like to thank R. G. Buchheit and H. O. Colijn for technical support, B.C. Pitts, F. Buehlmann and W. Zhang for supplying the samples, M. Caroselli for the SEM investigation.

References

1. Ishitani, T., Ohnishi, T., Madokoro, Y. & Kawanami, Y. (1991). Focused-ion-beam "cutter" and "attacher" for micromachining and device transplantation. *J. Vac. Sci. Technol B, 9*(5), p. 2633-2637. DOI: https://doi.org/10.1116/1.585661
2. Komano, H., H. Nakamura, T., & Takigava, T. (1991). A rewiring technique for integrated circuit operation analysis using a silicon oxide film deposited by focused ion beam. *J. Vac. Sci. Technol. B 9*(5), p. 2653-2655. DOI: https://doi.org/10.1116/1.585665
3. Nikawa, K. (1991). Applications of focused ion beam technique to failure analysis of very large scale integrations: a review. *J. Vac. Sci. Technol B, 9*(5), p. 2566-2577. DOI: https://doi.org/10.1116/1.585694
4. Kirk, E. C. G., McMahon, R. A., Cleaver, J. R. A. & Ahmed, H. (1988). Scanning ion microscopy and microsectioning of electron beam recrystallized silicon on insulator devices. *J. Vac. Sci. Technol. B, 6*(6), p. 1940-1944. DOI: https://doi.org/10.1116/1.584137
5. Young, R. J., Kirk, E. C. G., Williams, D. A. & Ahmed, H. (1990). Fabrication of Planar and Cross-Sectional TEM Specimens Using a Focused Ion Beam. *Mat. Res. Soc. Symp. Proc.,* 199, p. 205-216. https://link.springer.com/article/10.1557/PROC-199-205
6. 6. Kern, D. P., Lee, K. Y., Laibowitz, R. B. & Gupta, A. (1991). High resolution patterning of high Tc superconductors. J. Vac. Sci. Technol., B, 9(6), p. 2875-2878. DOI: https://doi.org/10.1116/1.585616
7. Presser, N. & Hilton, M. R. (1997). Applications of focused ion beam machining to the characterization of carbide, nitride and oxide films. Thin Solid Films, 308-309, 369-374. DOI: https://doi.org/10.1016/S0040-6090(97)00583-X
8. Davis, S. T. & Khamsehpour, B. (1996). Focused ion beam machining and deposition for nanofabrication. *Vacuum, 47*(5), p. 455-462. https://wrap.warwick.ac.uk/id/eprint/18850/
9. Heilmann, A., Altmann, F., Katzer, D., Müller, F., Sawitowski, Th. & Schmid, G. (1999). Determination of the pore size and the vertical structure of nanaporous aluminum oxide membranes. Applied Surface Science, 144-145, p. 682-685. DOI: https://doi.org/10.1016/S0169-4332(98)00899-X
10. Smith, A. J., Tran, T. & Wainwright, M. S. (1999). Kinetics and mechanism of the preparation of Raney® copper. Journal of Applied Electrochemistry, 29, p. 1085-1094. https://link.springer.com/article/10.1023/A:1003637410133
11. FEI Company, xP Dualbeam Workstation User' s Guide. Revolution Publishing, 2003
12. Material Safety Data Sheet for Alodine 1200S, Henkel Corp., Ed., Madison Heights, 1997.
13. Maissel, L. I. & Glang, R. (1970). Handbook of Thin Film Technology. McGraw-Hill. https://www.amazon.in/Handbook-Thin-Film-Technology-Maissel/dp/0070397422
14. Matsui, S. & Ochiai, Y. (1996). Focused ion beam applications to solid state devices. *Nanotechnology, 7*(3), p. 247-258. DOI: https://iopscience.iop.org/article/10.1088/0957-4484/7/3/013

15. Buchheit, R. G., Boger, R. K., Carroll, M. C., Leard, R. M., Paglia, C. S. & Searles, J. L. (2001). The electrochemistry of intermetallic particles and localized corrosion in Al alloys. *JOM, 53*(7), p. 29–33. https://link.springer.com/article/10.1007/s11837-001-0084-x
16. Buchheit R. G., Grant R. P., Hlava, P. F., McKenzie, B., & Zender, G. L. (1997). Local dissolution phenomena associated with S phase (Al2CuMg) particles in aluminum alloy 2024-T3. *J. Electrochem. Soc., 144*(8), p. 2621-2628. DOI: https://doi.org/10.1149/1.1837874
17. Obispo H. M., Murr, L. E., Arrowood, R. M. & Trillo, E. A. (2000). Copper deposition during the corrosion of aluminum alloy 2024 in sodium chloride solutions. *Journal of Materials Science*, 35, p. 3479-3495. https://link.springer.com/article/10.1023/A:1004840908494
18. Dimitrov, N., Mann, J. A., Vukmirovic, M., & Sieradzki, K. (2000). Dealloying of Al2CuMg in alkaline media. *Journal of the Electrochemical Society, 147*(9), p. 3283-3285. https://asu.elsevierpure.com/en/publications/dealloying-of-alsub2subcumg-in-alkaline-media
19. Wagner, K., Brankovic, S. R., Dimitrov, N., & Sieradzki, K. (1997). Dealloying below the critical potential. *J. Electrochem. Soc., 144*(10), p. 3545-3555. DOI: http://dx.doi.org/10.1149/1.1838046
20. Sieradzki, K. & Newman, R.C. (1987). Stress-corrosion cracking. *J. Phys. Chem. Solids, 48*(11), p. 1101-1113. DOI: https://doi.org/10.1016/0022-3697(87)90120-X
21. Li, R. & Sieradzki, K. (1992). Ductile-brittle transition in random porous Au. *Phys. Rev. Lett., 68*(8), p. 1168-1171. DOI: https://doi.org/10.1103/PhysRevLett.68.1168
22. Pitts, B. C., Paglia, C. S. & Buchheit, R. G. (in press). The Role of Anodic Dissolution in the Stress Corrosion Cracking of 7075-T6 (Al-5.6Zn-2.5Mg-0.23Cr) Aluminum Alloy (to be submitted for Corrosion journal).
23. Kendig, M., E. Addison, R. & Jeanjacquet, S. (1999). The Influence of Adsorbed Oxo-Cr(VI) Species on the Zeta Potential in the Porous Oxide of Anodized Aluminum. *J. Electrochem. Soc., 146*(12), p. 4419. https://iopscience.iop.org/article/10.1149/1.1392653
24. Llevbare, G. O., Scully, J. R., Yuan, J. & Kelly, R. G. (2000). Inhibition of Pitting Corrosion on Aluminum Alloy 2024-T3: Effect of Soluble Chromate Additions vs Chromate Conversion Coating. *Corrosion, 56*(3), 227-242. DOI: https://doi.org/10.5006/1.3287648
25. Pocock, W. E. (1954). Metal finishing, 52, p. 48.
26. Sakashita, M. & Sato, N. (1979). Corrosion, 35, p. 351. https://www.researchgate.net/publication/24340502_Electrochemical_Impedance_Spectroscopy_Of_Metal_Alloys
27. Sato, N. (1989). 1989 Whitney Award Lecture: Toward a More Fundamental Understanding of Corrosion Processes. *Corrosion, 45*(5), p. 354-368. DOI: https://doi.org/10.5006/1.3582030
28. Glass, A. L. (1968). Materials protection, 25.
29. Arrowsmith, D. J., Dennis, J. K. & Sliwinski, P.R. (1984). Trans. Inst. Met. Fin., 62, p. 117.
30. Treverton, J. A. & Davies, N.C. (1977). An XPS study of chromate pretreatment of aluminium. *Metals Tech., 4*(1), 480-489. DOI: https://doi.org/10.1179/030716977803292808
31. Judd, M. & Brindly, K. (1992). Soldering in electronics assembly. Newnes. https://api.pageplace.de/preview/DT0400.9780080517346_A24385752/preview-9780080517346_A24385752.pdf
32. Coombs, C. F. (1995). Printed Circuits Handbook.

Copyright: ©2025 Paglia, C. This is an open-access article distributed under the terms of the Creative Commons Attribution License, which permits unrestricted use, distribution, and reproduction in any medium, provided the original author and source are credited.